Chemical Science

ROYAL SOCIETY OF CHEMISTRY

EDGE ARTICLE

View Article Online
View Journal

Cite this: DOI: 10.1039/d6sc00713a

All publication charges for this article have been paid for by the Royal Society of Chemistry

Nano-visualization of hydrogel dynamics *via* surface plasmon-enhanced aggregation-induced emission

Qing-Bo Liang,†[a] Zhao Li,†[a] Yu-Hua Weng,[a] Lang Chang,[a] Jia-Dai Wang,[a] Ting-Bin Wen,[a] Shuo-Hui Cao*[abc] and Yao-Qun Li*[a]

Understanding conformational transitions in hydrogels is essential for deciphering their stimulus-responsive behavior, yet real-time, label-free monitoring at the nanoscale has remained a fundamental barrier. Here, we introduce surface plasmon coupling aggregation-induced emission (SPCAIE) as a new observational paradigm that enables *in situ* visualization of hydrogel dynamics with sub-nanometer axial displacement sensitivity. Our approach establishes a synergistic, label-free feedback loop between molecular conformation and optical output by merging the interfacial sensitivity of plasmonics with the microenvironmental responsiveness of non-covalently embedded AIE luminogens. This new transduction mechanism directly converts intrinsic nanoscale motions into quantifiable, amplified optical signals, overcoming the limitations of conventional invasive or ensemble-averaging techniques. The SPCAIE framework not only reveals previously inaccessible stimulus-induced rearrangements in hydrated environments, but also establishes a generalizable principle for probing soft matter interfaces. Our work provides a transformative conceptual and methodological platform for analyzing the dynamics of hydrated soft materials, with broad applicability to diverse stimulus-responsive polymer systems, opening new pathways in soft matter research and advanced material design.

Received 26th January 2026
Accepted 21st May 2026

DOI: 10.1039/d6sc00713a

rsc.li/chemical-science

Introduction

In recent decades, polymer and gel materials have experienced rapid development and widespread adoption, with advanced hydrogels emerging as particularly promising candidates. These materials exhibit exceptional tensile properties, including remarkable strain capacity, attributable to their distinctive hybrid network architectures. Furthermore, their mechanical performance can be precisely tailored by modulating the composition, concentration, and relative ratios of constituent components. Hydrogels represent a class of cross-linked polymeric materials featuring three-dimensional network structures that demonstrate exceptional water absorption capacity while preserving structural integrity without dissolution. Through sophisticated molecular design, researchers have developed stimuli-responsive hydrogels capable of sensing and responding to various environmental cues, including temperature fluctuations, pH variations, mechanical pressure, light exposure, electric fields, and magnetic fields.[1–7] These unique characteristics have propelled their extensive utilization across diverse applications, ranging from controlled drug delivery systems and tissue engineering scaffolds to advanced biosensing platforms.[8–13]

The swelling behavior of hydrogels—characterized by their reversible transition between collapsed and extended states and quantified through both equilibrium swelling ratios and kinetic swelling rates—represents a fundamental property governing hydrogel performance.[14] Precise characterization of these swelling dynamics is critical for the rational design of hydrogels tailored to specific applications.[15] Since swelling dynamics are intrinsically linked to dimensional changes, various analytical techniques have been developed to capture these variations, particularly in film thickness. Current techniques for probing hydrogel swelling, a key conformational transition, are largely limited to *ex situ* methods. Conventional approaches include spectroscopic ellipsometry,[16] scanning electron microscopy (SEM),[17] atomic force microscopy (AFM),[18] nuclear magnetic resonance,[19] and neutron reflectometry.[20] However, accurate nanoscale characterization of hydrogel thickness presents significant experimental challenges.[21] These *ex situ* techniques often require sample dehydration or complex modeling, which can alter or infer rather than directly capture hydrated, dynamic states. For instance, SEM requires freeze-drying or critical point drying to prevent the structural collapse of the three-

[a]*Department of Chemistry and the MOE Key Laboratory of Spectrochemical Analysis & Instrumentation, College of Chemistry and Chemical Engineering, Xiamen University, Xiamen 361005, P. R. China. E-mail: shuohuicao@xmu.edu.cn; yaoqunli@xmu.edu.cn*

[b]*Department of Electronic Science, Xiamen University, Xiamen 361005, P. R. China*

[c]*Shenzhen Research Institute of Xiamen University, P. R. China*

† These authors contributed equally to this work.

dimensional hydrogel network, while AFM imaging of hydrated soft materials demands exceptional tip performance to minimize imaging artifacts, and neutron scattering requires extensive data modeling and either prior structural knowledge or explicit assumptions about the hydrogel architecture.

Beyond those *ex situ* methods, several research efforts, including our own, have employed fluorescence-based techniques for *in situ* investigation of nanoscale environments within polymer materials.[22–25] Förster Resonance Energy Transfer (FRET)-based polymer brushes can monitor conformational transitions through specifically integrated donor–acceptor pairs, but they report only on intra- or inter-molecular distances within a narrow range (1–10 nm) and require covalent labeling, which limits material generality.[22] Autofluorescent polyelectrolytes avoid exogenous probes yet are restricted to specific polymer chemistries that exhibit native fluorescence, severely narrowing their applicability.[23] Our group previously introduced the angle scanning-surface plasmon coupled emission (AS-SPCE) technique for real-time monitoring of the growth process of fluorophore-labeled polymers;[24] however, SPCE alone still requires covalent labeling and, without an environmentally sensitive luminogen, cannot report on local chain packing or hydration independently of the emitter–interface distance. These techniques thus face a fundamental dilemma: they rely on specific, covalently attached fluorescent reporters that constrain material scope and introduce an unavoidable compromise between signal generation and measurement fidelity, as the label may perturb the native properties and interactions of the polymer. Thus, a transformative platform that combines non-invasive operation, nanoscale spatial resolution, and universal material compatibility has remained an outstanding challenge.

To overcome these challenges, we present surface plasmon coupling aggregation induced emission (SPCAIE), a strategy that integrates the axial ranging capability of SPCE with the microenvironmental sensitivity of AIE into a single measurement. The SPCE phenomenon arises from the interaction between fluorescent molecules and surface plasmon polaritons at the metal–dielectric interface,[26–29] providing exceptional spatial sensitivity through the exponential decay of plasmonic coupling intensity.[30–34] This SPCE platform can precisely quantify fluorophore displacement distance normal to the interface by analyzing the angular distribution and polarization state of the SPCE signal. Meanwhile, AIE luminogens (AIEgens) exhibit a photophysical behavior where molecular aggregation under a microenvironment restricts intermolecular motions (*e.g.*, rotation and vibration), resulting in greatly enhanced fluorescence.[35–40] The synergistic combination of these two effects in our work establishes the first non-invasive approach for monitoring polymer conformational transitions with simultaneous real-time temporal resolution and sub-nanometer axial displacement sensitivity. This work establishes SPCAIE not merely as a new technique, but as a conceptual and methodological framework that redefines the observation of soft matter interfaces. SPCAIE induces a label-free feedback loop: it leverages the material's intrinsic conformational change to modulate an AIE process, the emission of which is then dramatically amplified and spatially confined by surface plasmons. This direct, simultaneous delivery of both spatial and environmental information from an unlabeled sample represents a unique conceptual advance not achieved by previous techniques. This synergy directly transduces nanoscale mechanical motions into a quantitative, macroscopic optical readout with sub-nanometer axial displacement sensitivity, circumventing the traditional trade-off between non-invasiveness and sensitivity.

Results and discussion

As a proof-of-concept demonstration, we selected pH-responsive poly(acrylic acid)/poly(vinyl alcohol) (PAA/PVA) hydrogel ($pK_a \approx 4.5$)[41,42] as a model system. The AIEgens triphenylaminothiophene pyridine (TTPy) was facilely incorporated into the hydrogel matrix through simple mixing without covalent modification. Employing our AS-SPCE microscopy platform in the Kretschmann configuration, we successfully monitored hydrogel thickness variations in real time during pH stimulation by characterizing the SPCAIE response (Fig. 1). Below the pK_a, the collapsed hydrogel state restricts the intramolecular motion of TTPy, while above the pK_a, swelling leads to the restoration of intramolecular motion of TTPy within the polymer network. These structural transitions occur within the decay length of the interfacial evanescent field in SPCE. Remarkably, the system exhibits dual signal amplification mechanisms: first through distance-dependent SPCE effect that enables nanoscale thickness sensitivity at the interface, and second *via* the AIE effect that responds to microenvironmental changes during TTPy aggregation driven by polymer conformational transitions. The SPCAIE approach overcomes fundamental limitations of conventional methods by synergistically combining the nanoscale spatial precision of SPCE with the exceptional microenvironmental responsiveness of AIEgens, establishing a label-free, real-time paradigm for studying soft matter dynamics. The non-covalent incorporation of AIEgens offers material versatility beyond the PAA/PVA hydrogel system

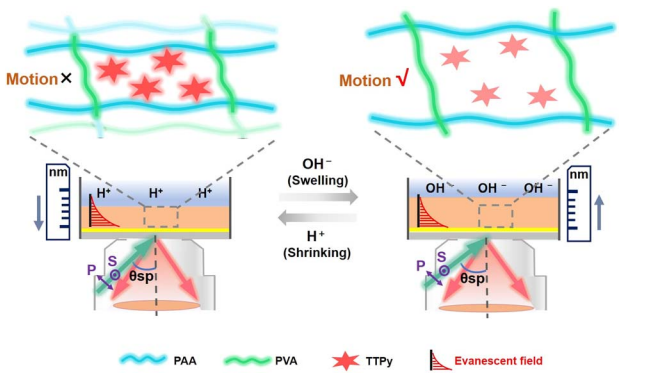

Fig. 1 Schematic illustration of real-time nanoscale monitoring of hydrogel conformational dynamics *via* surface plasmon-coupled aggregation-induced emission. A pH-responsive poly(acrylic acid)/poly(vinyl alcohol) (PAA/PVA) hydrogel incorporated with a triphenylaminothiophene pyridine (TTPy) molecular probe serves as the model system.

demonstrated here. We anticipate broad applicability of this platform across diverse stimuli-responsive polymers, enabling new opportunities in biological sensing, smart material development, and fundamental studies of polymer dynamics at the nanoscale.

The architectural configuration of the TTPy-incorporated hydrogel and the experimental setup of the AS-SPCE microscopy are illustrated in Fig. 2a, which enables reliable modulation of both polarization and excitation angle (see Fig. S1 for instrument details). TTPy was synthesized according to established methods[43] and characterized as shown in Fig. S2. Fluorescence measurements confirmed its AIE characteristics (Fig. S3). Efficient SPCE coupling is facilitated by the spectral overlap between the emission band of TTPy and the surface plasmon resonance (SPR) of the underlying gold substrate.[31,44] Structural analyses *via* FT-IR spectroscopy confirmed the successful formation of a cross-linked hydrogel network within the PAA/PVA matrix and importantly indicated that the incorporation of TTPy did not perturb the intrinsic chemical properties of the polymer blend (Fig. 2b). Furthermore, SEM imaging revealed a smooth and homogeneous morphology of the hydrogel (Fig. 2c), supporting reliable thickness characterization. The SPCAIE technique allows precise characterization of the fluorescent hydrogel film thickness through analysis of excitation angle distribution patterns, particularly leveraging the directional and polarization-dependent nature of SPCE. Validation studies demonstrated excellent agreement between SEM cross-sectional measurements (311 nm dry-state thickness) and SPCAIE-derived thickness values (see Fig. S4 for details), strongly underscoring the reliability and precision of this optical methodology. This integrated platform is particularly powerful for monitoring hydrogel swelling dynamics with nanoscale resolution, owing to its intrinsic compatibility with liquid-phase environments, thereby enabling real-time observation of polymer conformational changes under physiologically relevant hydrated conditions.

As demonstrated in Fig. S5a, incubation of the hydrogel in buffer solution (pH 6.0) yielded distinct optimal excitation angles—66.0° for p-polarization and 68.9° for s-polarization under laser excitation—corresponding to a swollen thickness of 498.5 nm. Variations in the solution pH (6.0, 6.5, and 6.8) induced measurable and systematic shifts in the angular distributions: the p-polarized angle shifted from 64.7° to 65.5°, whereas the s-polarized angle remained constant at 68.9° (Fig. 2d and e). These angular shifts correspond to a progressive increase in film thickness from 498.5 nm to 503.3 nm (Fig. S6). A pivotal advantage of polarization-resolved SPCAIE is its capacity to provide deep molecular-level insight into the hydrogel's structural reorganization during pH-induced conformational transitions. By simultaneously capturing emissions from perpendicular (p-polarized) and parallel (s-polarized) molecular dipoles relative to the metal interface, SPCE affords unique three-dimensional structural resolution,[45]

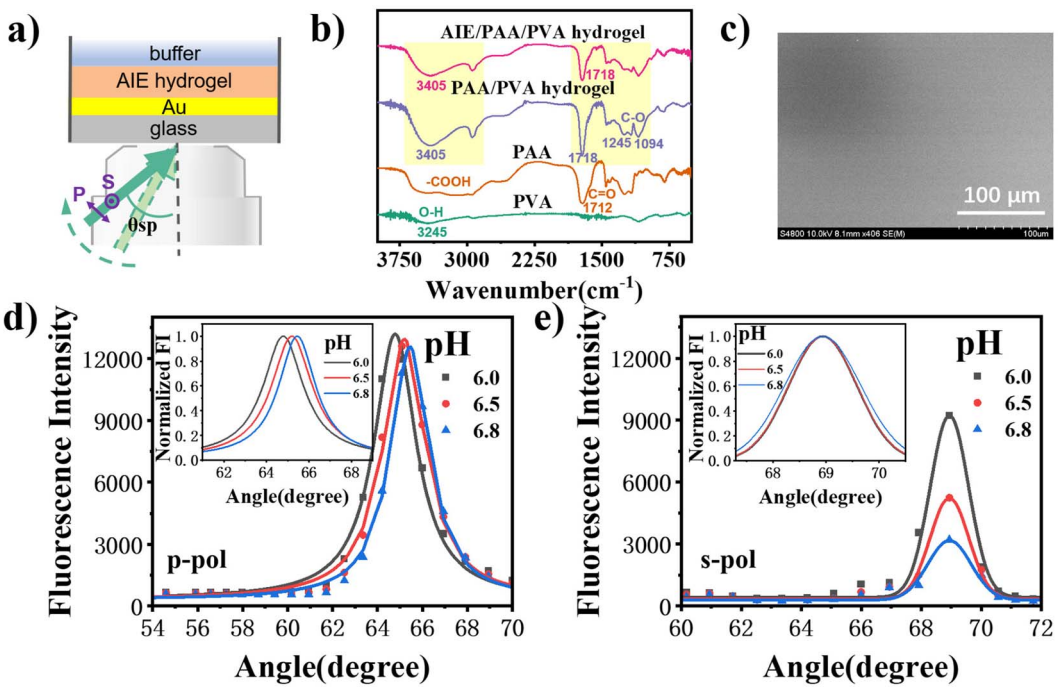

Fig. 2 Characterization of the AIE-incorporated hydrogel chip and its SPCE sensing performance. (a) Schematic of the SPCE experimental setup used for real-time hydrogel analysis. (b) FT-IR spectra of pure PAA, pure PVA, PAA/PVA hydrogel, and TTPy/PAA/PVA hydrogel, showing characteristic peaks at 1094 cm^{-1}, 1245 cm^{-1}, 1718 cm^{-1}, and 3405 cm^{-1}, confirming successful network formation. (c) SEM image of the TTPy/PAA/PVA hydrogel film spin-coated on a gold-coated coverslip (30 nm Au). (d) p-Polarized and (e) s-polarized excitation angular distributions measured by the AS-SPCE system at pH 6.0, 6.5, and 6.8, with incident angle scanned from 0° to 80°. Symbols represent experimental data; solid lines denote fitting results; insets display normalized fluorescence intensity as a function of incident angle.

which extends far beyond the thickness-only information accessible *via* conventional techniques such as ellipsometry.

The polarization-dependent responses offer particularly valuable insights into molecular orientation and dipole alignment within the swelling hydrogel. The more pronounced decrease in s-polarized SPCE intensity suggests significantly greater mobility and increased spatial separation among TTPy dipoles oriented parallel to the substrate surface during swelling. This anisotropic emission response reflects constrained swelling perpendicular to the film plane, with dimensional changes occurring predominantly along the thickness direction in spatially confined hydrogel films.[46,47] The persistence of s-polarized angle, coupled with intensity reduction, indicates that in-plane dipoles aligned parallel to the interface experience fewer restrictions and undergo more substantial rearrangement, whereas vertically aligned (p-polarized) out-of-plane dipoles are relatively constrained and more strongly influenced by the film's vertical expansion. Such discrimination between in-plane and out-of-plane molecular motions is not accessible by conventional thickness measurements (*e.g.*, ellipsometry or profilometry), highlighting the unique capability of SPCAIE to probe anisotropic chain dynamics within the hydrogel network. Given the enhanced sensitivity of s-polarized excitation to in-plane dipole rearrangements and its pronounced intensity response during swelling, it was selected as the standard mode for all subsequent experiments, providing optimal resolution for tracking molecular-scale reorganization during hydrogel transitions.

We propose that the SPCAIE signal arises from a synergistic combination of the aggregation-induced emission (AIE) effect and surface plasmon-coupled emission (SPCE). To decouple these contributions, we designed two control systems: a TTPy-incorporated hydrogel on a non-plasmonic glass substrate (exhibiting AIE only; Fig. 3d) and a conventional Rhodamine B (RhB)-doped hydrogel on a gold film (exhibiting SPCE only; Fig. 3g). Using our custom-built dual-mode AS-SPCE platform, which supports simultaneous spectral acquisition and spatial imaging, we systematically evaluated the fluorescence responses of all three systems across a range of physiologically relevant pH conditions (Fig. 3b, e and h). The PAA-based hydrogel exhibits pH-responsive swelling behavior governed primarily by the deprotonation of carboxyl groups along the polymer backbone. This process disrupts interchain hydrogen bonding and introduces electrostatic repulsion among ionized carboxylate groups, leading to network expansion.[48,49] Although these mechanisms collectively promote progressive swelling across the physiological pH range (6.5–7.4), the resultant volumetric changes remain constrained by the cross-linked network

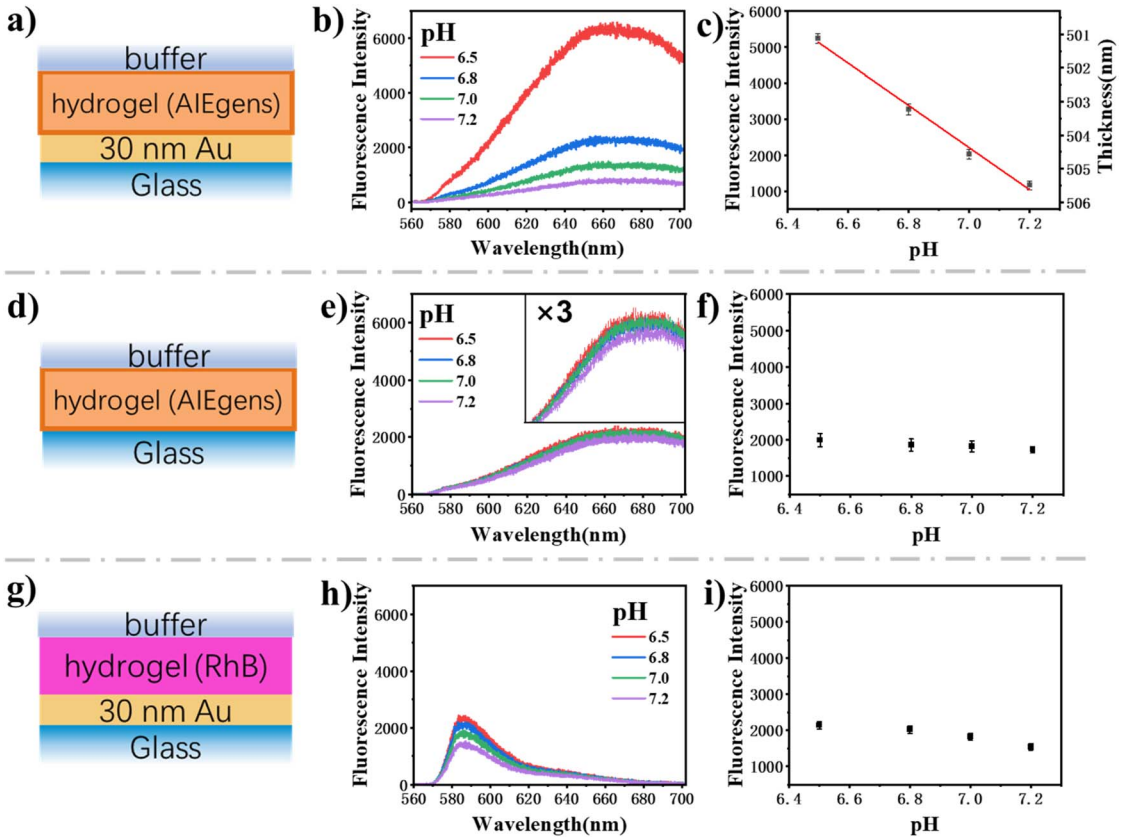

Fig. 3 Comparative analysis of the response characteristics for three systems. pH values of 6.5, 6.8, 7.0, and 7.2 were used for demonstration. (a–c) AIEgen-doped hydrogel on a gold substrate (combining both SPCE and AIE effects); (d–f) AIEgen-doped hydrogel on a non-plasmonic glass substrate (AIE effect only); and (g–i) RhB-doped hydrogel on a gold substrate (SPCE effect only). Each row presents schematic illustrations (a, d and g), corresponding emission spectra (b, e and h), and fluorescence intensity as a function of pH and film thickness ($N = 4$) (c, f and i).

structure. Crucially, the limited swelling magnitude proves insufficient to significantly alter either the spatial distribution of TTPy molecules within the evanescent field region (which critically governs SPCE coupling efficiency) or the molecular packing state of the AIEgen (which fundamentally dictates AIE intensity). Consequently, both control systems exhibited only modest fluorescence variations under identical pH stimuli (Fig. 3d and g).

In contrast, the SPCAIE system demonstrated dramatically enhanced signal modulation, exceeding the combined contributions of either AIE or SPCE operating independently (Fig. 3c). Despite the relatively limited absolute swelling degree, the system exhibited a responsivity slope more than 50-fold steeper than that of the control system on a glass substrate, endowing it with exceptional detection sensitivity. SPCAIE imaging further confirmed highly uniform signal distribution throughout the hydrogel matrix (Fig. S7), indicating that the AIEgens maintain stable integration within the polymer network without leaching during swelling. The absence of observable spectral shifts across all conditions (Fig. 3b and e) suggests that fluorescence intensity changes primarily stem from restricted intramolecular motion of the AIEgens, rather than from alterations in their aggregation state. This is supported by the control experiment (Fig. 3e), in which an AIE-active film (prepared under AIE-inducing conditions) exhibited only a weak pH response, confirming that the strong signal modulation observed in SPCAIE originates from the synergistic coupling effect rather than from the AIEgen's inherent sensitivity alone.

The exceptional sensitivity of SPCAIE is rooted in a synergistic dual-amplification mechanism, which constitutes the core conceptual advance of this work. This mechanism operates through a cascading process: first, the nanoscale swelling or contraction of the hydrogel network directly modulates the intramolecular motion (rotation/vibration) of the non-covalently embedded AIEgens. Second, this AIE emission is not passively collected but is actively and selectively amplified by SPCE effect. Specifically, the s-polarized SPCE component enhances emission from dipole moments oriented parallel to the metal interface, providing exquisite interfacial specificity and distance-dependent sensitivity. Critically, these two processes are not sequential but are intrinsically coupled, creating a coherent, label-free feedback loop. This loop directly and dynamically transduces minute conformational changes into a strongly amplified, quantifiable optical signal with exceptional signal-to-noise ratio and spatial precision, overcoming the historic trade-off between sensitivity and non-invasiveness in interfacial analysis. Owing to this foundational mechanism, the SPCAIE platform exhibits broad material compatibility and robust operability in liquid environments, establishing a generalizable paradigm for real-time interfacial science. Its utility extends far beyond the model hydrogel system, positioning it as a promising tool for real-time monitoring within complex chemical and biological settings, including biomarker detection, cellular microenvironment mapping, and dynamic analysis of soft matter transitions.

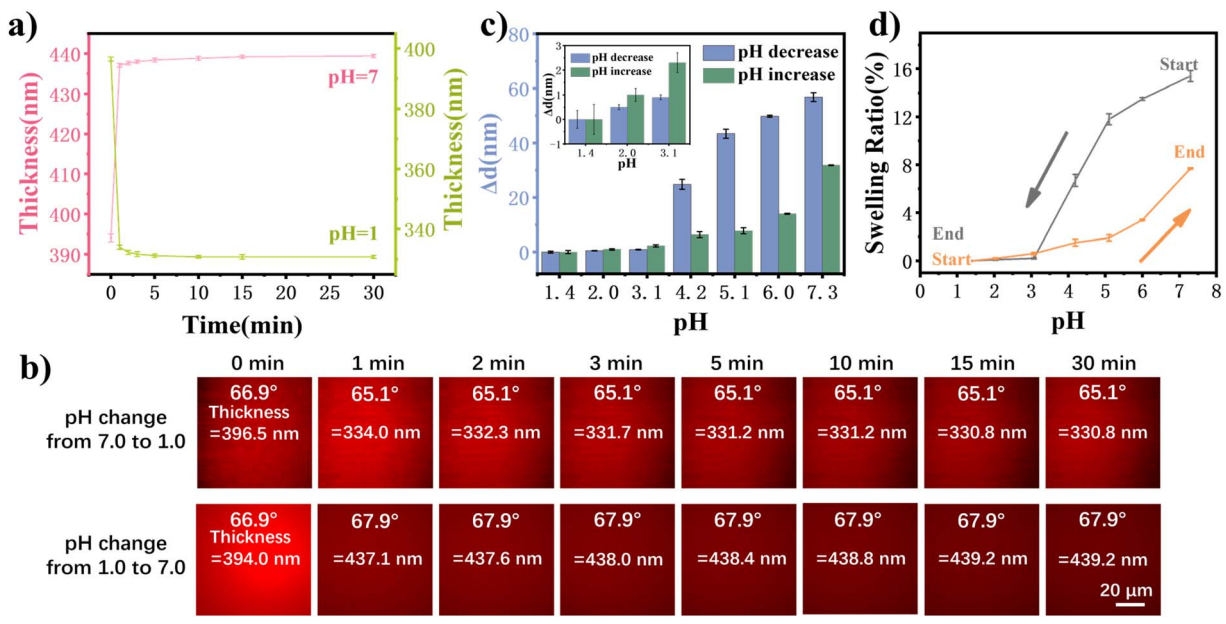

Fig. 4 pH-Dependent thickness variations of PAA/PVA hydrogel characterized by SPCAIE. (a) Real-time monitoring of hydrogel transient response during pH transitions between acidic (pH 1.0) and neutral (pH 7.0) conditions. Pink squares and olive circles separately denote transitions starting at pH 1.0 and at pH 7.0. (b) Corresponding fluorescence micrographs documenting the dynamic swelling/deswelling process. (c) Quantified thickness dynamics during pH cycling (the magnified inset revealing sub-nanometer resolution). pH-Dependent transitions are represented by blue columns (pH 7.3 to 1.4, deswelling) and green columns (pH 1.4 to 7.3, swelling). (d) pH-Cycling behavior showing swelling ratio hysteresis: gray curve represents neutral-to-acidic transition (pH 7.3 to 1.4); orange curve represents the reverse transition. All error bars represent mean ± standard deviation ($n = 3$). SPCE angles scanned from 0° to 80°; film thickness was obtained by fitting the angular reflectivity curves using a four-layer Fresnel model. pH was adjusted using buffer solutions.

To demonstrate its capability in resolving nanoscale dynamics, we characterized the hydrogel's real-time switching behavior through alternating exposure to acidic (pH 1.0) and neutral (pH 7.0) solutions. Transition from pH 1.0 to 7.0 was initiated by applying a microdroplet of acidic solution to the hydrogel surface, followed by rapid infusion of neutral buffer. The reverse transition (pH 7.0 to 1.0) was performed using an analogous exchange protocol. Real-time conformational dynamics were monitored *via* SPCAIE signal acquisition, with simultaneous recording of excitation angular distributions for comprehensive analysis (Fig. S9). As quantitatively summarized in Fig. 4a, the hydrogel exhibited rapid and reversible pH-responsive behavior. Both switching directions achieved detectable thickness changes within 1 minute and reached equilibrium within 3 minutes after pH alteration. Complementary SPCAIE imaging (Fig. 4b) provided spatial insight into swelling/deswelling dynamics, enabling direct correlation among fluorescence intensity, angular distribution profiles, and temporal evolution.

Notably, shifts in angular distributions—reflecting thickness variations on the tens-of-nanometer scale—were accompanied by synchronous fluorescence intensity changes sensitive to even subtler structural rearrangements. These dual optical signatures yielded distinct kinetic profiles for swelling and deswelling processes. Together, the results demonstrate the hydrogel's rapid response kinetics and high structural stability over multiple pH cycles. We attribute the fast-switching behavior to the highly hydrated nature of the nanoscale hydrogel film, which enables rapid hydration triggered by deprotonation (swelling) and efficient water expulsion during protonation (collapse), facilitating efficient conformational transitions between collapsed and swollen states.

To elucidate the conformational changes in detail, we systematically investigated the equilibrium swelling behavior of the hydrogel across a range of pH conditions. Quantitative analysis of both angular distribution and fluorescence intensity variations was performed during reversible transitions between acidic and neutral environments (Fig. S10). The results revealed asymmetric dimensional changes: swelling from pH 1.4 to 7.3 induced a 32 nm increase in thickness, while the reverse transition (pH 7.3 to 1.4) resulted in a more pronounced contraction of 57 nm (Fig. 4c). Since the hydrogel film is confined on a planar substrate, dimensional changes are restricted to the thickness direction (*z*-axis), enabling precise determination of the swelling ratio (SR) according to:

$$\mathrm{SR}\ (\%) = \left(\frac{d_t - d_0}{d_0}\right) \times 100$$

where d_0 and d_t denote the hydrogel film thickness at reference (pH 1.4) and test conditions during either forward or reverse pH transitions, respectively.

The pH-dependent swelling behavior is summarized in Fig. 4d. During the forward transition (pH 1.4 → 7.3), the SR increased continuously, with especially pronounced swelling above the pK_a of PAA. This behavior is attributed to carboxyl group ionization, where enhanced electrostatic repulsion promotes hydration, leading to marked hydrogel expansion. In contrast, the reverse transition (pH 7.3 → 1.4) exhibited a more complex SR profile, which can be divided into three distinct regions: (1) between pH 7.3 and 5.1, the hydrogel retained higher SR values relative to the fully collapsed state, showing gradual deswelling that reflects relaxation of the pre-expanded network; (2) near the pK_a region (pH 5.1–4.2), a rapid decrease in SR occurred due to reduced electrostatic repulsion and constraints from network elasticity as carboxyl groups became protonated; (3) below pH 3.1, complete protonation eliminated interchain repulsion, causing the SR to stabilize at a minimum value.

Notably, even in this plateau region, SPCAIE detected sub-nanometer thickness variations, confirming that the fully protonated state exhibits negligible swelling compared to the reverse transition (Fig. 4c, inset). The observed swelling–deswelling hysteresis—where forward and reverse pH transitions follow distinct SR pathways—is a characteristic behavior of ionic hydrogels, previously reported only at macroscopic scales.[50] In contrast to traditional methods that infer such hysteresis from ensemble-averaged bulk responses, SPCAIE directly resolves its nanoscale topography and dynamics in real time. To our knowledge, this work provides the first quantitative, *in situ* visualization of asymmetric nanoscale hydrogel dynamics with sub-nanometer axial displacement sensitivity, thereby bridging the critical gap between macroscopic property measurements and molecular-scale interactions. The SPCAIE technique thereby establishes a conceptually straightforward yet methodologically powerful platform for non-invasive, real-time interrogation of soft materials. Its superior *z*-axis spatial resolution, surpassing the diffraction limit and reaching the nanoscale, places it beyond the reach of conventional optical methods.[51]

Conclusions

In summary, this work establishes SPCAIE as a transformative paradigm for probing soft matter interfaces. By synergistically integrating the interfacial sensitivity of SPCE with the micro-environmental responsiveness of non-covalently embedded AIEgens, the SPCAIE platform not only achieves real-time, label-free visualization of nanoscale dynamics with exceptional spatiotemporal resolution, but also ensures non-invasiveness, experimental simplicity, and full compatibility with aqueous environments. The capability of this paradigm is decisively demonstrated through the resolution of a long-standing challenge: the first quantitative, *in situ* characterization of nanoscale swelling–deswelling hysteresis in ionic hydrogels. Moving beyond macroscopic averaging, SPCAIE captures this hysteresis with high fidelity, revealing the underlying interplay between network elasticity and electrostatic repulsion. It directly visualizes the suppression of swelling under protonated, hydrogen-bond-dominated conditions, providing mechanistic insight previously inaccessible.

Beyond these fundamental advances, the SPCAIE platform offers broad methodological versatility. Its high sensitivity, operational simplicity, and compatibility with hydrated environments position it as a powerful tool for studying hydration-

mediated processes in fields such as controlled drug delivery, soft actuators, and bio-integrated sensing. The underlying transduction principle, based on synergistic coupling of evanescent-field sensitivity with microenvironment-responsive emission, is generalizable to systems that satisfy three necessary conditions: optical transparency at the excitation and emission wavelengths, responsive conformational changes occurring within the evanescent-field penetration depth, and compatibility with non-covalent incorporation of AIEgens. The approach is readily adaptable to diverse stimuli-responsive polymers and can be extended to complex biological milieus—from polymer brushes and multilayer films to biomimetic membranes. In practice, successful translation also requires that the AIEgen remains stably entrapped without leaching over repeated stimulation cycles and that its loading does not perturb the intrinsic responsiveness of the matrix. Representative candidate systems include thermo-responsive polymers, polyelectrolyte brushes, and biopolymer networks. Thus, SPCAIE emerges not merely as an analytical technique, but as a generalizable framework for probing dynamic interfaces, paving the way for next-generation soft-matter design and interfacial science.

Author contributions

Q. B. L., Z. L., S. H. C., and Y. Q. L. designed the study and wrote the manuscript. Q. B. L. and Z. L. performed the majority of the experiments and analyzed the data. Y. H. W., L. C., and J. D. W. assisted with the fabrication and characterization of hydrogels. T. B. W. provided guidance on the preparation of AIE dyes. S. H. C. and Y. Q. L. conceived and supervised the project.

Conflicts of interest

There are no conflicts to declare.

Data availability

The authors declare that all the data are available within the article and its supplementary information (SI) or from the corresponding author upon reasonable request. Supplementary information: materials and methods, Fig. S1–S10. See DOI: https://doi.org/10.1039/d6sc00713a.

Acknowledgements

This work was supported by the National Natural Science Foundation of China (No. 22474121, 22274137, 22574139, 21974117), the Science and Technology Projects of Fujian Province (No. 2022Y4008), Natural Science Foundation of Fujian Province (No. 2026J010014), Natural Science Foundation of Xiamen (No. 3502Z202573021), the Basic and Applied Basic Research Foundation of Guangdong Province (No. 2024A1515011974), and Fundamental Research Funds for the Central Universities (No. 20720250071).

References

1 J. Yang, W. Huang, K. Peng, Z. Cheng, L. Lin, J. Yuan, Y. Sun, N.-J. Cho and Y. Chen, Versatile agar-zwitterion hybrid hydrogels for temperature self-sensing and electro-responsive actuation, *Adv. Funct. Mater.*, 2024, **34**, 2313725.
2 R. Cheng, M. Xu, X. Zhang, J. Jiang, Q. Zhang and Y. Zhao, Hydrogen bonding enables polymer hydrogels with pH-induced reversible dynamic responsive behaviors, *Angew. Chem., Int. Ed.*, 2023, **62**, e202302900.
3 G. Ge, Y. Zhang, J. Shao, W. Wang, W. Si, W. Huang and X. Dong, Stretchable, Transparent, and self-patterned hydrogel-based pressure sensor for human motions detection, *Adv. Funct. Mater.*, 2018, **28**, 1802576.
4 A. Meeks, M. M. Lerch, T. B. H. Schroeder, A. Shastri and J. Aizenberg, Spiropyran photoisomerization dynamics in multiresponsive hydrogels, *J. Am. Chem. Soc.*, 2022, **144**, 219–227.
5 Q. L. Zhu, C. Du, Y. Dai, M. Daab, M. Matejdes, J. Breu, W. Hong, Q. Zheng and Z. L. Wu, Light-steered locomotion of muscle-like hydrogel by self-coordinated shape change and friction modulation, *Nat. Commun.*, 2020, **11**, 5166.
6 J. H. Park, P. J. Grimes, H. E. Symons, N. Braidotti, S. Rochat, M. S. Workentin and P. Gobbo, Photochemical patterning and characterization of mechanical properties on soft materials, *Adv. Funct. Mater.*, 2025, **35**, 2416095.
7 R. Goodrich, Y. Tai, Z. Ye, Y. Yin and J. Nam, A Magneto-Responsive hydrogel system for the dynamic mechano-modulation of stem cell niche, *Adv. Funct. Mater.*, 2023, **33**, 2211288.
8 S. S. Liow, Q. Dou, D. Kai, Z. Li, S. Sugiarto, C. Y. Y. Yu, R. T. K. Kwok, X. Chen, Y.-L. Wu, S. T. Ong, A. Kizhakeyil, N. K. Verma, B. Z. Tang and X. J. Loh, Long-term real-time *in vivo* drug release monitoring with AIE thermogelling polymer, *Small*, 2017, **13**, 1603404.
9 K. Mendez, W. Whyte, B. R. Freedman, Y. Fan, C. E. Varela, M. Singh, J. C. Cintron-Cruz, S. E. Rothenbücher, J. Li, D. J. Mooney and E. T. Roche, Mechanoresponsive drug release from a flexible, tissue-adherent, hybrid hydrogel actuator, *Adv. Mater.*, 2024, **36**, 2303301.
10 N. D. Caprio, M. D. Davidson, A. C. Daly and J. A. Burdick, Injectable MSC spheroid and microgel granular composites for engineering tissue, *Adv. Mater.*, 2024, **36**, 2312226.
11 Y. Kittel, L. P. B. Guerzoni, C. Itzin, D. Rommel, M. Mork, C. Bastard, B. Häßel, A. Omidinia-Anarkoli, S. P. Centeno, T. Haraszti, K. Kim, J. Guck, A. J. C. Kuehne and L. De Laporte, Varying the stiffness and diffusivity of rod-shaped microgels independently through their molecular building blocks, *Angew. Chem., Int. Ed.*, 2023, **62**, e202309779.
12 F. Keyvani, H. Zheng, M. R. Kaysir, D. F. Mantaila, P. Ghavami Nejad, F. A. Rahman, J. Quadrilatero, D. Ban and M. Poudineh, A hydrogel microneedle assay combined with nucleic acid probes for on-site detection of small molecules and proteins, *Angew. Chem., Int. Ed.*, 2023, **62**, e202301624.

13 M. H. Ayoubi-Joshaghani, K. Seidi, M. Azizi, M. Jaymand, T. Javaheri, R. Jahanban-Esfahlan and M. R. Hamblin, Potential applications of advanced nano/hydrogels in biomedicine: static, dynamic, multi-stage, and bioinspired, *Adv. Funct. Mater.*, 2020, **30**, 2004098.

14 T. Jayaramudu, H.-U. Ko, H. C. Kim, J. W. Kim and J. Kim, Swelling behavior of polyacrylamide–cellulose nanocrystal hydrogels: swelling kinetics, temperature, and pH Effects, *Materials*, 2019, **12**, 2080.

15 J. Tavakoli, H. P. Zhang, B. Z. Tang and Y. Tang, Aggregation-induced emission lights up the swelling process: a new technique for swelling characterisation of hydrogels, *Mater. Chem. Front.*, 2019, **3**, 664–667.

16 W. Ogieglo, H. Wormeester, K.-J. Eichhorn, M. Wessling and N. E. Benes, In situ ellipsometry studies on swelling of thin polymer films: A review, *Prog. Polym. Sci.*, 2015, **42**, 42–78.

17 V. B. Schwartz, F. Thétiot, S. Ritz, S. Pütz, L. Choritz, A. Lappas, R. Förch, K. Landfester and U. Jonas, Antibacterial surface coatings from zinc oxide nanoparticles embedded in poly(N-isopropylacrylamide) hydrogel surface layers, *Adv. Funct. Mater.*, 2012, **22**, 2376–2386.

18 Y. Dong, E. M. Akinoglu, H. Zhang, F. Maasoumi, J. Zhou and P. Mulvaney, An optically responsive soft etalon based on ultrathin cellulose hydrogels, *Adv. Funct. Mater.*, 2019, **29**, 1904290.

19 R. Wang, J. Xin, Z. Ji, M. Zhu, Y. Yu and M. Xu, Spin-space-encoding magnetic resonance imaging: a new application for rapid and sensitive monitoring of dynamic swelling of confined hydrogels, *Molecules*, 2023, **28**, 3116.

20 A. Vidyasagar, J. Majewski and R. Toomey, Temperature induced volume-phase transitions in surface-tethered poly(N-isopropylacrylamide) networks, *Macromolecules*, 2008, **41**, 919–924.

21 V. S. Raghuwanshi and G. Garnier, Characterisation of hydrogels: Linking the nano to the microscale, *Adv. Colloid Interface Sci.*, 2019, **274**, 102044.

22 Q. A. Besford, H. Yong, H. Merlitz, A. J. Christofferson, J.-U. Sommer, P. Uhlmann and A. Fery, FRET-integrated polymer brushes for spatially resolved sensing of changes in polymer conformation, *Angew. Chem., Int. Ed.*, 2021, **60**, 16600–16606.

23 G. Aktas Eken, Y. Huang, Y. Guo and C. Ober, Visualization of the pH response through autofluorescent poly(styrene-alt-N-maleimide) polyelectrolyte brushes, *ACS Appl. Polym. Mater.*, 2023, **5**, 1613–1623.

24 Y.-H. Weng, L.-T. Xu, M. Chen, Y.-Y. Zhai, Y. Zhao, S. K. Ghorai, X.-H. Pan, S.-H. Cao and Y.-Q. Li, In situ monitoring of fluorescent polymer brushes by angle-scanning based surface plasmon coupled emission, *ACS Macro Lett.*, 2019, **8**, 223–227.

25 X. Wu and C. Barner-Kowollik, Fluorescence-readout as a powerful macromolecular characterisation tool, *Chem. Sci.*, 2023, **14**, 12815–12849.

26 S. Rathnakumar, S. Bhaskar, V. Sivaramakrishnan, N. S. V. Kambhampati, V. Srinivasan and S. S. Ramamurthy, Tecoma stans floral extract-based biosynthesis for enhanced surface plasmon-coupled emission and a preliminary study on fluoroimmunoassay, *Anal. Chem.*, 2024, **96**, 4005–4012.

27 S. Bhaskar, D. Thacharakkal, S. S. Ramamurthy and C. Subramaniam, Metal–dielectric interfacial engineering with mesoporous nano-carbon florets for 1000-fold fluorescence enhancements: smartphone-enabled visual detection of perindopril erbumine at a single-molecular level, *ACS Sustainable Chem. Eng.*, 2023, **11**, 78–91.

28 J. S. Yuk, E. F. Guignon and M. A. Lynes, Sensitivity enhancement of a grating-based surface plasmon-coupled emission (SPCE) biosensor chip using gold thickness, *Chem. Phys. Lett.*, 2014, **591**, 5–9.

29 J. M. Rice, L. J. Stern, E. F. Guignon, D. A. Lawrence and M. A. Lynes, Antigen-specific T cell phenotyping microarrays using grating coupled surface plasmon resonance imaging and surface plasmon coupled emission, *Biosens. Bioelectron.*, 2012, **31**, 264–269.

30 C. D. Geddes, I. Gryczynski, J. Malicka, Z. Gryczynski and J. R. Lakowicz, Directional surface plasmon coupled emission, *J. Fluoresc.*, 2004, **14**, 119.

31 S. H. Cao, W. P. Cai, Q. Liu and Y. Q. Li, Surface plasmon–coupled emission: what can directional fluorescence bring to the analytical sciences?, *Annu. Rev. Anal. Chem.*, 2012, **5**, 317–336.

32 Z. Gryczynski, J. Borejdo, N. Calander, E. Matveeva and I. Gryczynski, Minimization of detection volume by surface-plasmon-coupled emission, *Anal. Biochem.*, 2006, **356**, 125–131.

33 Q. Su, C. Jiang, D. Gou and Y. Long, Surface plasmon-assisted fluorescence enhancing and quenching: From theory to application, *ACS Appl. Bio Mater.*, 2021, **4**, 4684–4705.

34 M. Chen, S. H. Cao and Y. Q. Li, Surface plasmon–coupled emission imaging for biological applications, *Anal. Bioanal. Chem.*, 2020, **412**, 6085–6100.

35 W. Lu, S. Wei, H. Shi, X. Le, G. Yin and T. Chen, Progress in aggregation-induced emission-active fluorescent polymeric hydrogels, *Aggregate*, 2021, **2**, e37.

36 M. Luo, S. Wang, C. Li, W. Miao and X. Ma, Aggregation-induced emission organogel formed by both sonication and thermal processing based on tetraphenylethylene and cholesterol derivative, *Dyes Pigm.*, 2019, **165**, 436–443.

37 Z. Wang, J. Nie, W. Qin, Q. Hu and B. Z. Tang, Gelation process visualized by aggregation-induced emission fluorogens, *Nat. Commun.*, 2016, **7**, 12033.

38 T. Han, C. Gui, J. W. Y. Lam, M. Jiang, N. Xie, R. T. K. Kwok and B. Z. Tang, High-contrast visualization and differentiation of microphase separation in polymer blends by fluorescent AIE probes, *Macromolecules*, 2017, **50**, 5807–5815.

39 S. Satapathy, P. Prabakaran and E. Prasad, Augmenting photoinduced charge transport in a single-component gel system: controlled *in situ* gel–crystal transformation at room temperature, *Chem.–Eur. J.*, 2018, **24**, 6217–6230.

40 Y. Ren, S. Xie, E. Svensson Grape, A. K. Inge and O. Ramström, Multistimuli-responsive enaminitrile

molecular switches displaying H^+-induced aggregate emission, metal ion-induced turn-on fluorescence, and organogelation properties, *J. Am. Chem. Soc.*, 2018, **140**, 13640–13643.

41 G. Gerlach, M. Guenther, J. Sorber, G. Suchaneck, K.-F. Arndt and A. Richter, Chemical and pH sensors based on the swelling behavior of hydrogels, *Sens. Actuators, B*, 2005, **111–112**, 555–561.

42 M. D. Kurkuri and T. M. Aminabhavi, Poly(vinyl alcohol) and poly(acrylic acid) sequential interpenetrating network pH-sensitive microspheres for the delivery of diclofenac sodium to the intestine, *J. Controlled Release*, 2004, **96**, 9–20.

43 D. Wang, M. M. S. Lee, G. Shan, R. T. K. Kwok, J. W. Y. Lam, H. Su, Y. Cai and B. Z. Tang, Highly efficient photosensitizers with far-red/near-infrared aggregation-induced emission for *in vitro* and *in vivo* cancer theranostics, *Adv. Mater.*, 2018, **30**, 1802105.

44 I. Gryczynski, J. Malicka, Z. Gryczynski and J. R. Lakowicz, Surface plasmon-coupled emission with gold films, *J. Phys. Chem. B*, 2004, **108**, 12568–12574.

45 Y. Zhao, Y.-H. Liu, S.-H. Cao, M. Ajmal, Y.-Y. Zhai, X.-H. Pan, M. Chen and Y.-Q. Li, Excitation–emission synchronization-mediated directional fluorescence: insight into plasmon-coupled emission at vibrational resolution, *J. Phys. Chem. Lett.*, 2020, **11**, 2701–2707.

46 M. E. Harmon, T. A. M. Jakob, W. Knoll and C. W. Frank, A surface plasmon resonance study of volume phase transitions in n-isopropylacrylamide gel films, *Macromolecules*, 2002, **35**, 5999–6004.

47 I. Tokarev and S. Minko, Stimuli-responsive hydrogel thin films, *Soft Matter*, 2009, **5**, 511–524.

48 K.-F. Arndt, A. Richter, S. Ludwig, J. Zimmermann, J. Kressler, D. Kuckling and H.-J. Adler, Poly(vinyl alcohol)/poly(acrylic acid) hydrogels: FT-IR spectroscopic characterization of crosslinking reaction and work at transition point, *Acta Polym.*, 1999, **50**, 383–390.

49 J. Sorber, G. Steiner, V. Schulz, M. Guenther, G. Gerlach, R. Salzer and K.-F. Arndt, Hydrogel-based piezoresistive pH sensors: investigations using FT-IR attenuated total reflection spectroscopic imaging, *Anal. Chem.*, 2008, **80**, 2957–2962.

50 A. Richter, A. Bund, M. Keller and K.-F. Arndt, Characterization of a microgravimetric sensor based on pH sensitive hydrogels, *Sens. Actuators, B*, 2004, **99**, 579–585.

51 Q. A. Besford, P. Uhlmann and A. Fery, Spatially resolving polymer brush conformation: opportunities ahead, *Macromol. Chem. Phys.*, 2023, **224**, 2200180.